THEORETICAL & APPLIED MECHANICS LETTERS **2**, 031006 (2012)

Fatigue life assessment of a high strength steel 300 M in the gigacycle regime

Hongqian Xue,[a)] Pingli Liu, Peng Chen, and Jie Wang
School of Mechatronics Northwestern Polytechnical University, Xi'an 710072, China

(Received 18 March 2012; accepted 2 April 2012; published online 10 May 2012)

Abstract The fatigue behavior of a high strength steel 300 M in the gigacycle regime was investigated. Fully reversed tension – compression fatigue tests at ambient temperature were performed using an ultrasonic fatigue system operating at 20 kHz. The staircase test method was employed to obtain accurate values of the mean fatigue strength corresponding to fixed numbers of cycles up to 10^9. These results were compared to the curve which is estimated by the data tested in the mid-long life regime on conventional servo hydraulic test machine at 20 Hz. Results indicate that the fatigue strength determined from ultrasonic fatigue testing is lightly higher than conventional testing in the range of 10^6–10^7 cycles. It is obvious that nucleations of fractures tend to occur below the surface, if fractures happen after more than 10^7 cycles. All the fractured specimens fails from internal SiO_2 inclusions or smaller carbides and carbide clusters. [doi:10.1063/2.1203106]

Keywords 300 M steel, gigacycle fatigue, ultrasonic fatigue, very high cycle fatigue

Ultrasonic fatigue testing has received considerable attention in the last two decades. This is mainly due to the increasing use of engineering materials in applications with service lives reaching up to 10^9 load cycles.[1–3] The high strength steel 300 M as a kind of typical material is used as mechanical components in aircraft engineering, the design lives are required to extend into the super-long life range up to 10^9 cycles. In this case, probabilistic S–N curves including the super-long life regime are the basis for structural fatigue reliability assessment and life prediction.

It is well known that there is no fatigue limit for high-strength steels, as a rule, the S–N curve of high strength steel tested by rotary bending fatigue test system has two knee points (Fig. 1), which is different from the curves observed in common steel.[4,5] The different S–N curves characterized in high strength steel can be attributed to the transition of the fracture modes, that is, fatigue crack initiation site changes from surface to interior type in very high cycle fatigue region. However, another type of S–N curve of high strength steels that does not exhibit similar duplex S–N curves in very high cycle regime, has been reported.[6,7] High strength steel 100C6 is a typical steel that its S–N curve exhibits a continuous decrease in fatigue strength between fatigue lives of 10^6 and 10^9 cycles under cyclic uniaxial loading at room temperature.[7] It is pointed out that microstructure inhomogeneity and inclusion could be the potential sources of micro-crack.[7] However, the correlation between the subsurface crack initiation and fatigue strength is still not clear. The purpose of this investigation is therefore to evaluate the fatigue strength of 300 M steel in very high cycle regime and get a better understanding of the mechanisms of fatigue crack initiation.

a)Corresponding author. Email: xuedang@nwpu.edu.cn.

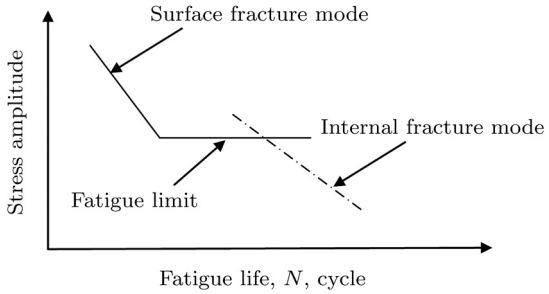

Fig. 1. Schematic representation of the duplex S–N curve for high strength steel tested by rotary bending fatigue test machine.[4]

The high strength steel 300 M studied in this work is a wrought cold work tool steel, chemical composition as derived from X-ray fluorescence analysis is shown for major elements in Table 1. All specimens were machined to the desired geometry and their surface longitudinally ground before the heat treatment. The steel was then quenched in oil at 975°C and tempering was done at 300°C for 2 h. Relatively high tempering temperature and slow subsequent cooling was chosen in order to lower quench-induced residual stresses and minimize thermal stresses in the specimens. Static strength properties measured are: ultimate tensile strength $R_m = 1\,800 \pm 20$ MPa, fracture strain $A_5 = 9.3\%$ and Young's modulus $E = 200$ GPa.

An ultrasonic fatigue machine and a conventional hydraulic servo fatigue machine (INSTRON8801) were used to determine the fatigue properties of 300 M steel in very high cycle regime and low cycle regime, respectively. The ultrasonic fatigue systems and their applications have been reviewed in some papers.[2–5]

The specimens used in ultrasonic fatigue test were cylindrical dog bones with a gage section diameter of

Table 1. Chemical composition of the testing material (wt/%).

C	Mn	Si	*S*	*P*	Ni	Cr	*V*	Al	Cu	Fe
0.38	0.76–0.9	1.51–1.7	0.03	0.007 5–0.008 5	1.8–1.9	0.85	0.07–0.08	0.4	0.07	rest

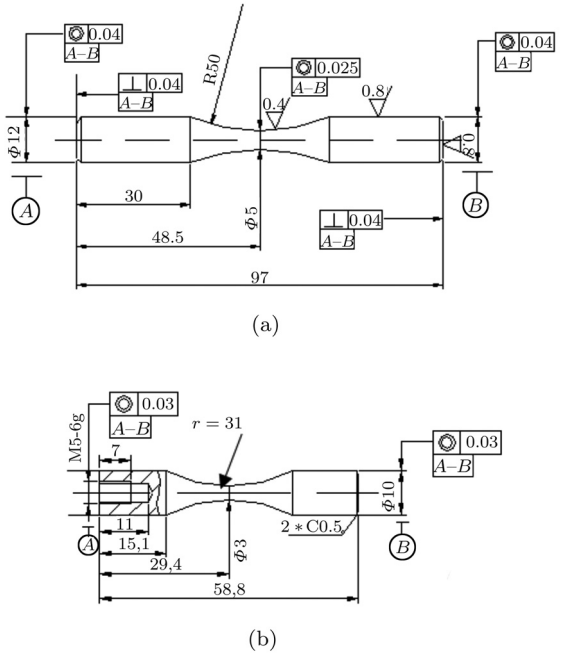

Fig. 2. Dimensions of the specimens used in (a) conventional fatigue test and (b) ultrasonic fatigue test.

3 mm. The specimens were designed so that the maximum strain is located in the gage section. The geometry of ultrasonic specimen and conventional fatigue specimen are shown in Fig. 2, respectively.

Conventional fatigue test was carried out on an INSTRON8801 fatigue test machine at a frequency of 20 Hz to measure the S–N data in mid-long life regime, applying a group test methods at 5 stress levels in S–N testing. Ultrasonic fatigue test with limited set of data was conducted to obtain fatigue limit up to 10^9 cycles using a staircase method.

In this study, all testing was performed at a stress ratio, $R = -1$. One of the greatest challenges of ultrasonic fatigue testing is measurement of the applied stress in the material. For that, an optical displacement sensor was used to measure displacement at the free end of a standard specimen. This displacement was calibrated with the gage section strain before test. The displacement, with the calibration factor, was then used during the testing to actively control the strain, and therefore the stress in the gage section. Besides, an important consideration in ultrasonic testing is the heat that can be generated internally due to internal friction and damping for the high strength steel, this internal damping can lead to large temperature increases, so it

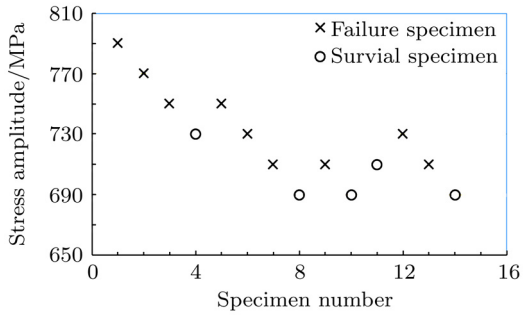

Fig. 3. Plot of staircase testing results of 300 M steel generated at 20 kHz.

should pay more attention to minimize the effects of the damping. In this test, the temperature in the specimen gage section was monitored by an infrared pyrometer, and the calibration factor in the room and elevated temperature was determined.

Fatigue properties of the high strength steel explained by S–N curves are plotted in Fig. 3. They show the elastic nominal peak stress of the specimen versus the number of cycles to failure. A test was considered a run-out if it lasted 10^6 cycles for conventional fatigue test, and the specimens, which did not fail, are marked with arrowhead. The fatigue life diagram could also be presented in the form of a Wohler-type S–N plot

$$\sigma_{\mathrm{a}} = \sigma'_{\mathrm{f}}(N_{\mathrm{f}})^b. \tag{1}$$

Equation (1) may be used to specify the approximation lines, i.e. the correlation of number of cycles, N and stress amplitudes, σ_{a}. Exponents b and constants σ_{f} for the approximation line are -0.0585 and 1 936, respectively. The mean fatigue limit at 10^6 cycles (50% fracture probability) is 830 MPa.

Very high cycle fatigue data measured under ultrasonic fully reversed tension–compression fatigue loading and using the staircase method described above are shown in Fig. 3. The specimens, fatigue crack initiated from subsurface, are marked with circle, and the specimens, fatigue crack initiated from surface, are marked with square. In the ultrasonic fatigue test using the staircase method, a stress of 790 MPa was chosen for initial tests based on 10^6 cycle fatigue limit results from the conventional fatigue S–N curve. When a specimen in the ultrasonic system failed at less than 10^9 cycles, the maximum stress was decreased by 20 MPa for the following test according to the staircase methodology. If the specimen did not fail in 10^9 cycles, the maximum stress was increased by 20 MPa for the subsequent test.

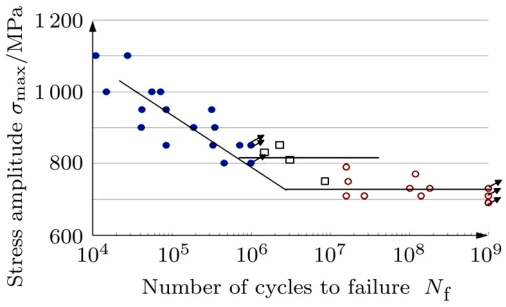

Fig. 4. Comparison of results from ultrasonic and conventional test systems.

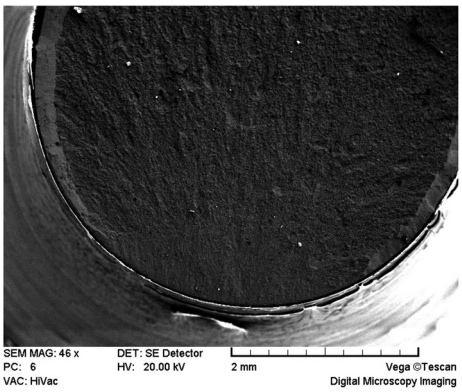

Fig. 5. Surface-originating fracture tested at 20 Hz (σ_{max} = 950 MPa, $N_f = 8.6 \times 10^4$).

The results of the staircase testing graphically are shown in Fig. 4. It shows that many specimens were failed over 10^7 cycles and also three specimens failed over 10^8 cycles. At very high numbers of cycles, fatigue data are approximated with a line parallel to the abscissa, which indicates the mean endurance limit at 10^9 cycles of 723 ± 22 MPa. The results tested at 20 kHz are compared with the low cycle fatigue using conventional fatigue testing machine, it exhibits apparent difference, the fatigue strength determined from ultrasonic fatigue testing was a litter higher than conventional testing around 10^6 cycles, the difference may be due to the lack of overlapping data at stresses of 850–750 MPa in the range of 10^5–10^7 cycles.

Figure 5 shows a typical fracture surface for the 300 M steel specimen from conventional fatigue testing at 20 Hz, the crack initiation points were all from surface, due to material surface scratches or cavities produced during grinding. However, fatigue crack initiations were mainly the sub-surface for fatigue specimens failed in very high cycle regime obtained at 20 kHz using ultrasonic fatigue system. This is consistent with the results of other high strength steel reported in many papers[5–8] that fatigue crack initiated from interior inclusions in very high cycle regime, no matter what the testing condition is. In contrast, for the specimens with lower fatigue life, fatigue crack mainly initiated from specimen surface.

Figure 6 shows typical fracture surfaces at around the fish-eye fracture origin. Most of the fish-eye fracture initiations were SiO_2 inclusions, and the sizes of the SiO_2 inclusion sizes in diameter ranged from 11 to 32 μm. However, in a few cases, the fish-eye fracture origins revealed no nonmetallic inclusion, as seen in Fig.6(b). In these cases, the fish-eye fracture initiation was the carbides and carbide clusters. Chemical compositions in the fatigue initiation region for two fractured specimens are shown in Table 2.

The fatigue strength shows a clear dependency on the dimension of the interior inclusion, i.e. the bigger interior inclusion has lower fatigue strength. Specially, it has greater fatigue strength with smaller carbides and carbide clusters. The fatigue lives were estimated at around 710 MPa, the fatigue life was 1.18×10^7 cycles

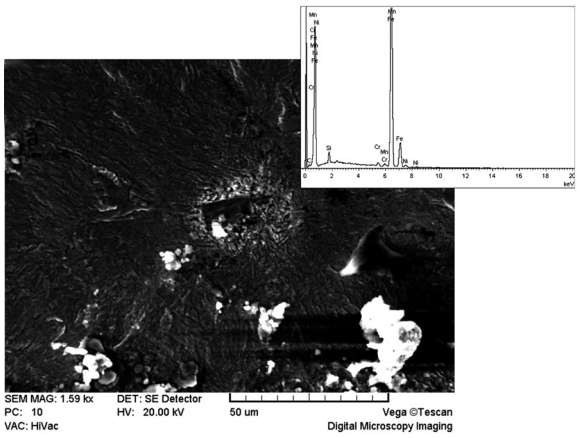

(a) SiO_2 inclusion

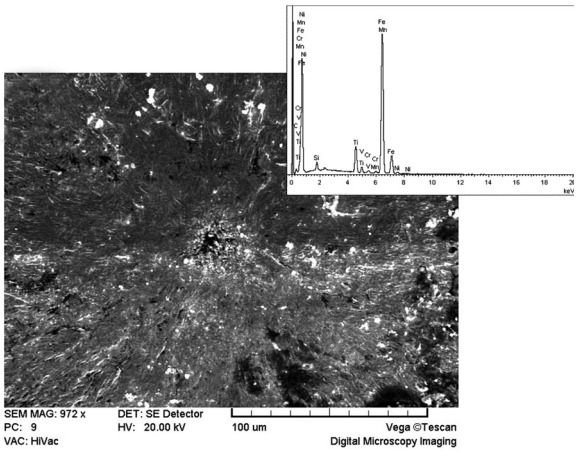

(b) Carbide clusters

Fig. 6. Fracture surface in interior inclusion induced fracture with a fish-eye.

Table 2. Chemical elements mass fraction in different points of crack initiation region (wt%).

	C	Si	S	O	Cr	Mn	Fe	Ni	V	total	
Point 1	0.30	90.84	1.24	5.37			2.25			100	In the rectangle
Point 2	0.09	1.75			0.91	0.96	94.53	1.74		100	of Fig. 6(a)
Point 1	0.23	1.64			0.76	0.78	86.15	8.19	0.84	100	In the circle
Point 2	1.04			23.82	0.94	0.67	20.52	43.22	3.02	100	of Fig. 6(b)

for the specimen with nonmetallic inclusion in diameter of 18.8 μm, in contrast to 1.06×10^8 cycles for the specimen with carbides and carbide clusters in diameter of 13.1 μm (Fig. 6).

In this study, several crack nucleation sites were small carbides and carbide clusters, located at the subsurface region, as shown in Fig. 6(b), instead, the occurrence of surface crack origins in tool steels was reported earlier.[9] The experimental findings clearly support the statistical estimations which proposed failures to start at the defect particles in very high cycle regime. Near-surface cracks originated at carbides/carbide clusters which just touch the surface or are located just below the surface, offering highest stress concentration. If corrosion caused by humidity is definitely a point of concern, fatigue crack tends to initiate at surface as the cited.[10] However, in this study an ultrasonic fatigue testing system was employed, consequently, testing times were several orders of magnitude shorter than in the cited study.[10] So, fatigue crack tended to initiate at the subsurface defect of this high strength steel in the absence of the influences of corrosion caused by humidity.

Primary carbides were found to have fractured at the entire fracture surface, and also the carbides at the crack origin were broken by SEM observations. Hard nonmetallic inclusions SiO_2 debonding might also be part of fatigue crack formation for the high strength steel 300 M.

Comparing with the S–N data obtained by conventional servo hydraulic fatigue testing at 20 Hz using large specimens with a straight section, ultrasonic fatigue testing technique was used to determine S–N data and fatigue limit using staircase method. The following conclusions may be drawn:

(1) High strength steel 300M showed a pronounced decrease in the slope of the S–N curve from 10^6 to 10^8 cycles. Five specimens failed above 10^8 cycles, the mean endurance limit at 10^7 cycles is only slightly (maximum 6%) higher than the mean endurance limit at 10^9 cycles.

(2) Internal failure have always started at SiO_2 inclusions in the center of the formed fish-eye, according to the presented statistical estimations, also some internal fish-eye failures of carbide clusters were experimentally obtained.

(3) Specimens without significant nonmetallic inclusion showed predominantly failure due to cracks originating subsurface small carbides and carbide clusters. Carbide particles were found fractured at the entire fracture surface.

This work was supported by the National Natural Science Foundation of China (50775182) and the Scientific Research Foundation for the Returned Overseas Chinese Scholars, State Education Ministry.

1. Q. Y. Wang, et al., Fatigue Fract. Eng. Mater. Struct. **8**, 662 (1999).
2. C. Bathias, Int. J. Fatigue **28**, 1438 (2006).
3. Y. Furuya, H. Hirukawa, and T. Kimura, et al., Metal. Trans. A **38**A, 1722 (2007).
4. Y. Murakami, N. N. Yokoyama, and J. Nagata, Fatigue Fract. Engng. Mater. Struct. **25**, 735 (2002).
5. Q. Y. Wang, C. Bathias, and N. Kawagoishi, et al., Int. J. Fatigue **24**, 1269 (2002).
6. V. Kazymyrovych, J. Bergstrom, and F. Thuvander, Int. J. Fatigue **32**, 1669 (2010).
7. C. Bathias, L. Drouillac, and P. Le Francois, Int. J. Fatigue **23**, 143 (2001).
8. H. Q. Xue, E. Bayraktar, and C. Bathias, J. Mater. Proc. Tech. **202**, 216 (2008).
9. Ryan J. Morrissey, and J. Patrick, Int. J. Fatigue **29**, 2079 (2007).
10. K. Tokaji, H. N. Ko, and M. Nakajima, et al., Mater. Sci. Engng. A **345**, 197 (2003).